The energy partition of underwater sparks

Randy M. Roberts, Jeffrey A. Cook, and Robert L. Rogers
University of Texas, Applied Research Laboratories, Austin, Texas 78713-8029

Austin M. Gleeson and Thomas A. Griffy
University of Texas, Department of Physics, Austin, Texas 78712-1081 and University of Texas,
Applied Research Laboratories, Austin, Texas 78713-8029

Underwater sparks have long been used by the geophysical prospecting community as a source of intense low-frequency sound. While bubble hydrodynamic models are well developed, the mechanism of transferring energy from the thermal power input, through the various energy conversion channels, to the work done by the bubble has not been adequately studied. In this work an *ab initio* model of the bubble dynamics, including blackbody ablation, ionization, dissociation, and radiative transport, is developed. This model is a first step in enumerating the important physical mechanisms within bubbles generated by underwater sparks. The predictions of this model are compared with experimental results. Experimental work is still needed to validate the model, and to determine if and how model parameters related to actual physical parameters and measurable effects. © *1996 Acoustical Society of America.*

INTRODUCTION

The underwater spark is being investigated as a practical source of low-frequency, high intensity underwater sound[1–6] which could serve as an alternative to the detonation of underwater explosives[7–11] and high pressure airguns.[12] The controllability and repeatability of underwater sparks are the principal advantages of these sound sources over underwater explosives. Since the efficiency of the spark sound source is a very important factor in the acceptance of underwater sparks as a practical sound source, there is a need to understand how the electrical energy from the spark is converted into acoustic radiation.

This paper deals with the thermodynamics of a spark generated underwater bubble during the early stages of the bubble's development. Our main purpose is to identify the energy conversion processes from the electrical energy of the spark into other channels, such as the internal energy of the gas, mechanical work, blackbody radiation, and acoustic radiation.

The spark occurs when electrical power is delivered to an arc that creates a bubble, which subsequently expands and collapses. The spark duration is much shorter than the period of the bubble's expansion and subsequent collapse. During the early stages of the bubble's growth, the temperatures and pressures inside the bubble become very high, and the conversion from electrical to mechanical energy takes place. Thus we expect the greatest effects on the efficiency of the sound source to occur during this early phase, when the temperatures are large and the bubble is small. We, therefore, have limited the scope of the model to times much shorter than the bubble period. On these time scales, experience shows that thermal power profiles are determined by the electrical circuit configuration and parameters. It is thus reasonable to take the thermal power delivered from the external energy delivery system as a given.

Because of the very large temperatures produced by the spark, we must incorporate the effects of dissociation, ionization, and blackbody radiation into the model of the bubble's development. Here we treat the bubble as a homogeneous globe of gas composed of a reacting mixture of water with its dissociated and ionized components to obtain a functional form for the internal energy of the gas within the bubble. We use the functional form for the internal energy to account for the flow of mass, from the surrounding water into the bubble, due to the blackbody radiation ablating the water from the bubble wall. The resulting model is then used to predict the acoustic radiation generated by the bubble.

The rest of this paper is divided into six sections. Section I describes the model that we have chosen to determine the growth of the bubble from the pressure and its rate of change within the bubble. In Sec. II we discuss how the rate of change of the temperature and pressure are determined from the internal energy function. Section III shows how an internal energy function that takes dissociation and ionization into account is determined. Blackbody radiation and its resulting ablation of the bubble wall are discussed in Secs. IV and V. Finally, Sec. VI displays results from the model, and compares the calculations to experimental results.

I. BUBBLE GROWTH MODEL

In order to model the growth of the bubble, we need a set of equations which relates the acceleration of the bubble wall to the ambient pressure in the surrounding water, the pressure within the bubble, and the time derivative of the pressure. The method that we use for determining the bubble wall acceleration is the Kirkwood–Bethe model,[8,7,13,12,1] originally used in the study of underwater explosions and airgun generated bubbles.[12]

The equation defining the radial bubble wall acceleration $\ddot{R}$ in terms of pressure at the bubble wall P and its time derivative $\dot{P}$ is[1]

$$\ddot{R}\left(1-\frac{\dot{R}}{C}\right)=\frac{\dot{P}}{\rho C}\left(1-\frac{\dot{R}}{C}\right)+\frac{H}{R}\left(1+\frac{\dot{R}}{C}\right)$$
$$-\frac{3}{2}\frac{\dot{R}^2}{R}\left(1-\frac{\dot{R}}{3C}\right), \tag{1}$$

where C and ρ are the speed of sound and the density of the water at the bubble wall, and H is the specific enthalpy at the bubble wall. (Uppercase variable names R, P, C, and H refer to values calculated at the bubble wall.) The specific enthalpy is defined for a given pressure p with respect to the ambient pressure p_0 by

$$h(p)=\int_{p_0}^{p}\frac{dp'}{\rho(p')}. \tag{2}$$

The specific enthalpy at the bubble wall is then

$$H=h(P). \tag{3}$$

The speed of sound and the density of the water at the bubble wall are functions of the pressure at the bubble wall. The speed of sound is calculated from the isentropic sound propagation condition,

$$c^2(p)=\left(\frac{\partial p}{\partial p}\right)_s, \tag{4}$$

$$C=c(P). \tag{5}$$

The functional form of $\rho(p)$ used in the Kirkwood–Bethe model is the Tait equation of state,

$$\left(\frac{p+B}{p_0+B}\right)=\left(\frac{\rho}{\rho_0}\right)^n, \tag{6}$$

with B, ρ_0, and n as constants, chosen to be 3000 atm, 1020 k/m^3, and 7, respectively. The ambient pressure of the surrounding water p_0 is dependent on the depth of the spark source beneath the surface.

It is evident from Eq. (1) that the radial acceleration of the bubble wall depends on the value of the pressure P and its time derivative $\dot{P}$. We must therefore have a means of calculating the time derivative of the pressure from knowledge of the heat and mass transport between the bubble and its surroundings.

II. TIME DERIVATIVES OF PRESSURE AND TEMPERATURE

Since we are assuming a homogeneous bubble and are neglecting surface tension, the pressure at the bubble wall P is the same as the pressure within the bubble. The problem of finding $\dot{P}$ becomes one of determining the rate of change of the internal pressure of the bubble with heat and mass transport taken into account. Since it will be necessary to keep track of the internal temperature of the bubble as well as the pressure, we must also find an expression for the time derivative of the temperature within the bubble $\dot{T}$, again taking into account heat and mass transport. Given an equation of state for the gas within the bubble we can calculate $\dot{P}$ from $\dot{T}$.

In this section we shall assume we know the total heat flow into the bubble $\dot{Q}$, the particle flow into the bubble $\dot{N}$,
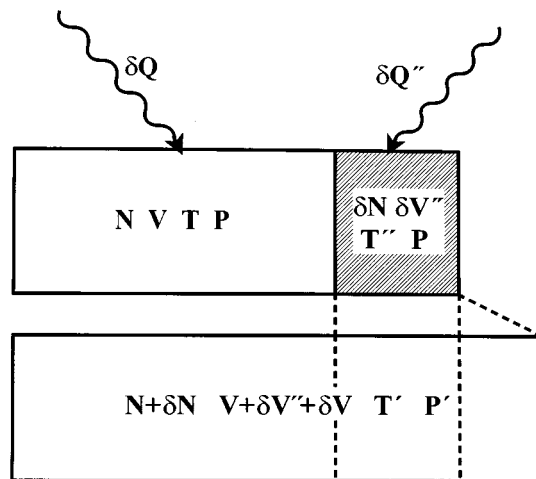

FIG. 1. The particle flow mechanism for a bubble in contact with the surrounding water. The top left rectangle represents the bubble at the beginning of the process. The shaded rectangle represents the water to be added irreversibly during the process. The bottom rectangle represents the bubble at the end of the process. The bubble has changed its volume due to the added mass and any work done to the surrounding water.

and the rate of change of the bubble's volume $\dot{V}$. We shall also assume we know how the internal energy of the gas depends on the number of water molecules, volume, and temperature of the bubble, i.e.,

$$E=E(N,V,T).$$

We show how to derive such a function in Sec. III.

Before describing the derivation of $\dot{T}$, and hence $\dot{P}$, it is necessary to explicitly consider the mechanisms which change the thermodynamic state of the bubble. In the evolution of the bubble, three mechanisms are responsible for changes of thermodynamic state: external heating or cooling of the bubble, work being done on or by the bubble, and mass flowing from the surrounding water into the bubble. These changes are illustrated in Fig. 1. In this diagram the top left rectangle illustrates the bubble at the beginning of the process of heating, mass flow, and work. The bubble is shown in contact with a small amount of water, illustrated by the shaded rectangle to its right. After this water is heated by an amount $\delta Q''$, it will be irreversibly added to the bubble. The details of this process are discussed in Sec. V. The total volume of the system consisting of the bubble and the small amount of water is $V+\delta V''$.

The lower rectangle represents the bubble at the end of the process, a time δt later. During this small time, an amount of heat δQ has been added to the bubble, and it has performed enough work on the surrounding water to change the total volume of the system by δV to $V+\delta V''+\delta V$. As a result of these changes, the temperature of the bubble has changed by δT, the number of water molecules by δN, the volume of the bubble by $\delta V''+\delta V$, and the pressure by δP.

The total energy of the system, consisting of both the bubble and the small amount of water, at the beginning of the time period is the sum of the energy of the bubble plus the energy of the small amount of water E'',

$$E_t=E(N,V,T)+E''. \tag{7}$$

The energy at the end of the time period is only the energy of the bubble,

$$E'_t = E(N + \delta N, V + \delta V'' + \delta V, T + \delta T). \quad (8)$$

If we assume all changes are small compared to their original values, we may determine the energy at the end of the time period to first order in the changes,

$$E'_t = E(N, V, T) + E_N \delta N + E_V \delta V'' + E_V \delta V + E_T \delta T. \quad (9)$$

Here E_N represents the partial derivative of E with respect to N holding V and T constant. The expressions for E_V and E_T are likewise defined.

The values of the energy before and after the time period are related by the first law of thermodynamics; therefore,

$$E'_t = E_t + \delta Q + \delta Q'' - P \delta V. \quad (10)$$

Equating Eqs. (7), (9), and (10), we arrive at an expression for δT,

$$E_T \delta T = E'' = \delta Q'' + \delta Q - P \delta V - E_N \delta N - E_V \delta V''$$
$$- E_V \delta V. \quad (11)$$

We now assume that $\delta Q''$ is the exact amount of heat needed to boil the δN molecules of water to a gas at the boiling point T_b and total energy $c_{vb} T_b \delta N$. Here c_{vb} is the specific heat per molecule for steam at its boiling point. The final expression for δT is

$$E_T \delta T = \left(c_{vb} T_b - E_N - \frac{1}{n_w} E_V \right) \delta N - (P + E_V) \delta V + \delta Q. \quad (12)$$

In the above equation we have replaced the volume of the water $\delta V''$ with by $(1/n_w) \delta N$, where n_w is the number density of the water surrounding the bubble, since we will be expressing the particle flow into the bubble by the number of molecules, not the volume, of added water. When we take the limit $\delta t \rightarrow 0$, we arrive at an expression for $\dot{T}$ in terms of the particle flow $\dot{N}$, the heat flow $\dot{Q}$, and the volume rate of change $\dot{V}$,

$$N c_v \dot{T} = \left(c_{vb} T_b - E_N - \frac{1}{n_w} E_V \right) \dot{N} - (P + E_V) \dot{V} + \dot{Q}. \quad (13)$$

In the above equation we have used the definition of the specific heat per molecule,

$$c_v = \frac{1}{N} E_T. \quad (14)$$

We can use the equation of state to obtain an expression for $\dot{P}$, which is needed by the bubble growth model. For a reacting mixture of ideal gases, the equation of state can be written as

$$PV = NTg(P, T). \quad (15)$$

The function $g(P, T)$ represents the ratio of the *actual* number of particles to the original number of water molecules tracked by the model. it is discussed further in Sec. III.

Again assuming all changes are small compared to their original values for the small time period δt, the change in pressure is related to other known changes by

$$\frac{\delta P}{P} \left[1 - \frac{P}{g} \left(\frac{\partial g}{\partial P} \right)_T \right] = \frac{\delta T}{T} \left[1 + \frac{T}{g} \left(\frac{\partial g}{\partial T} \right)_P \right]$$
$$+ \frac{\delta N}{N} \left(1 - \frac{n}{n_w} \right) - \frac{\delta V}{V}, \quad (16)$$

where $n = N/V$ is the number density of the hot gas. In the limit $\delta t \rightarrow 0$ the above equation becomes
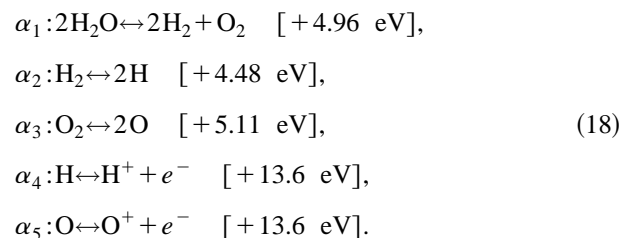
$$\frac{\dot{P}}{P} \left[1 - \frac{P}{g} \left(\frac{\Omega g}{\partial P} \right)_T \right] = \frac{\dot{T}}{T} \left[1 + \frac{T}{g} \left(\frac{\partial g}{\partial T} \right)_P \right]$$
$$+ \frac{\dot{N}}{N} \left(1 - \frac{n}{n_w} \right) - \frac{\dot{V}}{V}. \quad (17)$$

III. INTERNAL ENERGY FUNCTION

The previous section assumes that the internal energy of the gas is a known function of the number of water molecules, the volume of the bubble, and the temperature of the gas. In Eq. (15) we introduce a function of the pressure and temperature $g(P, T)$ into the equation of state. In this section we describe how to obtain expressions for these two functions by treating the gas within the bubble as an equilibrium configuration of a reacting mixture of water molecules with their dissociated and ionized components.

In the simulations we have run, we have determined that temperatures within the bubble can reach in excess of 10 000 K. At these temperatures water vapor no longer behaves as an ideal gas with constant specific heat; water dissociates into atomic hydrogen and oxygen. Ionization of hydrogen and oxygen can begin at temperatures of this order, as well. The dissociation and ionization processes influence the way heat is converted into work by diverting heat from raising the temperature of the bubble into changing the degree of dissociation and ionization. This diversion of heat from raising the temperature of the bubble can be seen through an increase in the specific heat of the system. We will show that the dissociation and ionization phase transitions are marked by a sharp peak in the specific heat.

The method used for analyzing the equilibrium state of a reacting mixture of ideal gases follows Landau and Lifshitz. (See Chap. X of Landau and Lifshitz.[14]) Five reactions describe the dissociation of water and the subsequent ionization of its atomic components,

$$\alpha_1 : 2H_2O \leftrightarrow 2H_2 + O_2 \quad [+4.96 \text{ eV}],$$
$$\alpha_2 : H_2 \leftrightarrow 2H \quad [+4.48 \text{ eV}],$$
$$\alpha_3 : O_2 \leftrightarrow 2O \quad [+5.11 \text{ eV}], \quad (18)$$
$$\alpha_4 : H \leftrightarrow H^+ + e^- \quad [+13.6 \text{ eV}],$$
$$\alpha_5 : O \leftrightarrow O^+ + e^- \quad [+13.6 \text{ eV}].$$

Each of these five reactions has an associated α_i, with $0 \leq \alpha_i \leq 1$, which parameterizes the completeness of the reaction proceeding from left to right. For example, when $\alpha_1 = 0$ the equilibrium configuration of the system would consist entirely of H_2O; when $\alpha_1 = 1$ all of the H_2O in the system would have broken down into H_2 and O_2, which could fur-

TABLE I. The chemical species and specific heats related to the j subscript.

				j				
	1	2	3	4	5	6	7	8
A_j	H_2O	H_2	O_2	H	O	H^+	O^+	e^-
c_{vj}	3	7/2	7/2	3/2	3/2	3/2	3/	3/2
c_{pj}	4	9/2	9/2	5/2	5/2	5/2	5/2	5/2

ther break down through the second and third reactions, etc. The number of each species present in the equilibrium configuration N_j can be related to the original number of water molecules N and the set of α_i parameters $\boldsymbol{\alpha}$ by

$$N_j = n_j(\boldsymbol{\alpha})N. \tag{19}$$

The functional form for the $n_j(\boldsymbol{\alpha})$ can be determined from the chemical reaction equations, e.g., $n_2(\boldsymbol{\alpha}) = \alpha_1(1-\alpha_2)$, and the total number of particles can, in turn, be related to $\boldsymbol{\alpha}$ and the original number of water molecules,

$$\bar{N} = \sum_j N_j = \sum_j n_j n_j(\boldsymbol{\alpha})N \tag{20}$$

$$= g(\boldsymbol{\alpha})N. \tag{21}$$

The $g(\boldsymbol{\alpha})$ in the above equation will later become the $g(P,T)$ introduced into the equation of state in Sec. II.

The chemical reactions in Eq. (18) can be written in compact form as

$$\sum_j \nu_{ij} A_j = 0 \quad \text{(for all } i\text{)}, \tag{22}$$

where the i runs over the number of chemical reactions, and j runs over the number of chemical species; in this case i runs from 1 to 5, and j runs from 1 to 8. The A_j are the symbols for the chemical species, e.g., H_2O or O, and ν_{ij} represent the stoichiometry of the reactions. The A_j's are listed in Table I, and the ν_{ij}'s are listed in Table II.

The required equilibrium conditions for a set of chemical reactions, described in the above form, are

$$\sum_j \nu_{ij} \mu_j = 0 \quad \text{(for all } i\text{)}, \tag{23}$$

where μ_j is the chemical potential for the jth chemical species at the given temperature and pressure.

For a mixture of ideal gases the chemical potential for the jth species in the mixture μ_j is (see Secs. 93, 42, and 43 of Landau and Lifshitz[14])

$$\mu_j = T \log P_j + \epsilon_{0j} - c_{pj} T \log T - T \eta_j, \tag{24}$$

TABLE II. The stoichiometric coefficients ν_{ij} for dissociation of water.

				j				
i	1	2	3	4	5	6	7	8
1	2	−2	−1	0	0	0	0	0
2	0	1	0	−2	0	0	0	0
3	0	0	1	0	−2	0	0	0
4	0	0	0	1	0	−1	0	−1
5	0	0	0	0	1	0	−1	−1

where P_j is the partial pressure, ϵ_{0j} is the ground-state energy per molecule, η_j is a constant related to the partition function that depends on the fundamental properties of the chemical species, and c_{pj} is the specific heat at constant pressure per molecule for the jth species. (In the following discussions the specific heat of a species is assumed constant. When the specific heat is a function of temperature we chose a specific heat value for the temperature near the expected dissociation temperature.) The values of specific heats which were used[14] are shown in Table I. This equation appears to be taking logarithms of dimensional quantities, but the η_j term contains logarithmic factors that cause the units to cancel.

Combining Eqs. (23) and (24), we arrive at a set of equations, one for each chemical reaction, that relate the partial pressures of the chemicals to the system's temperature:

$$\prod_j P_j^{\nu_{ij}} = \exp\left(\sum_j \nu_{ij}\eta_j\right) T^{\Pi_j \nu_{ij} c_{pj}} \exp\left(\frac{U_i}{T}\right). \tag{25}$$

We have substituted $U_i = \Pi_j \nu_{ij} \epsilon_{0j}$ into the above equation where U_i is the energy of reaction shown to the right of the ith chemical reaction in Eq. (18).

The partial pressure of the jth species P_j is the total pressure times the ratio of the number of the jth species to the total number of particles, i.e.,

$$\dot{P}_j = P \frac{N_j}{\bar{N}} \tag{26}$$

$$= P \frac{n_j(\boldsymbol{\alpha})}{g(\boldsymbol{\alpha})}, \tag{27}$$

which is just the pressure times a rational function of the α_i's. Therefore, the set of equations (25) represents five nonlinear equations with five unknown α_i's parameterized by the pressure and temperature of the system. Each nonlinear equation is of the following form:

$$F_i(\boldsymbol{\alpha})g(\boldsymbol{\alpha}) = PK_i(T) \quad \text{(for all } i\text{)}, \tag{28}$$

where F_i and K_i are known functions of their respective arguments determined from Eqs. (25) and (27). These nonlinear equations can be solved numerically to find the α_i's at a given pressure and temperature,

$$\alpha_i = \alpha_i(P,T). \tag{29}$$

Now it becomes evident that

$$g(\boldsymbol{\alpha}) = g(\boldsymbol{\alpha}(P,T)) = g(P,T), \tag{30}$$

and our equation of state for a mixture of ideal gases with a total of $\bar{N}$ particles becomes

$$PV = \bar{N}T \tag{31}$$

$$= NTg(P,T). \tag{32}$$

A plot of $g(P,T)$ vs T at $P = 1$ atm is shown in Fig. 2.

It is apparent from Eq. (17) that the derivatives of $g(P,T)$ are necessary to the calculation of $\dot{P}$ from $\dot{T}$. It is therefore necessary to derive expressions for the derivatives of α_i with respect to P and T. By taking the derivative of the
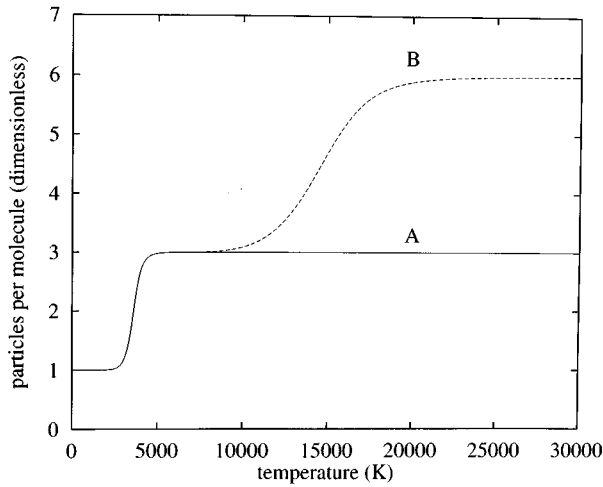
FIG. 2. The number of particles per water molecule versus temperature at 1 atm for dissociation only (A) and dissociation with ionization (B).

FIG. 3. The specific heat at constant volume per water molecule versus temperature at various pressures, (a) 1, (b) 10, (c) 100, and (d) 1000 atm.

set of equations (28) with respect to T, holding P constant, we arrive at a matrix equation that can be solved for the derivatives of the α_i's,

$$\sum_j \left(F_i(\boldsymbol{\alpha}) \frac{\partial g}{\partial \alpha_j} + \frac{\partial F_i}{\partial \alpha_j} g(\boldsymbol{\alpha}) \right) \left(\frac{\partial \alpha_j}{\partial T} \right)_P = P \frac{dK_i}{dT}. \quad (33)$$

A similar set of equations arises from the derivative with respect to P.

Without much difficulty the equation of state, Eq. (32), can be used to reformulate the nonlinear set of equations (25) in terms of N, V, and T. These equations can then be solved for the α_i's as a function of the number of original water molecules, the volume of the bubble, and the temperature of the bubble. In the same way as before, we can take derivatives of these nonlinear equations in order to determine the partial derivatives of the α_i's with respect to N, V, or T. In this way, were we to find an expression for the internal energy of the gas in terms of the α_i's, we would be able to calculate the derivatives of the energy necessary to calculate $\dot{T}$ from Eq. (13).

The total energy of the system is the sum of the energies of each constituent

$$E = \sum_j E_j. \quad (34)$$

Each constituent is modeled as an ideal gas with energy

$$E_j = N_j(c_{vj}T + \epsilon_{0j}). \quad (35)$$

We can express the total internal energy of the gas as a function of the number of original water molecules, the temperature, and the α_i's by combining the above equations

$$E = N \sum_j n_j(\boldsymbol{\alpha})(c_{vj}T + \epsilon_{0j}) \quad (36)$$

$$= N \left(\sum_j n_j(\boldsymbol{\alpha}) c_{vj} T + \sum_i u_i(\boldsymbol{\alpha}) U_i + \epsilon_{01} \right), \quad (37)$$

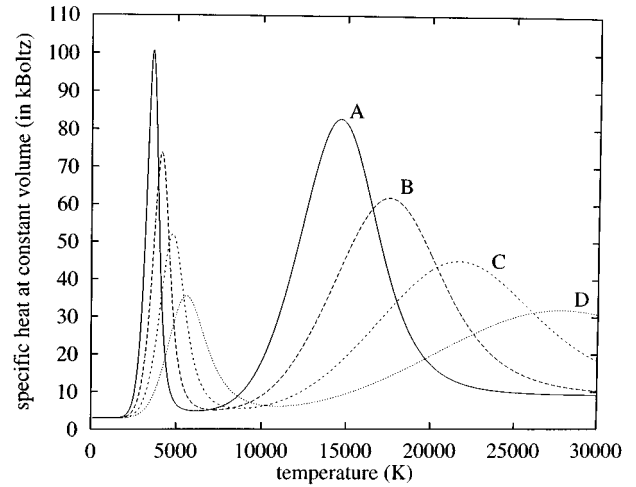$$E = E(N, T, \boldsymbol{\alpha}(N, V, T)) = E(N, V, T). \quad (38)$$

The $u_i(\boldsymbol{\alpha})$ are easily determined by contemplating the chemical reaction Eq. (18). It is easier to obtain the energy of reactions U_i than to come up with values for each of the ϵ_{0j}. Since the zero of energy is arbitrary, ϵ_{01} is chosen to be zero without loss of generality.

Since we have a method for calculating $\alpha_i(N, V, T)$, along with its partial derivatives, we have obtained a function for the internal energy of the gas with in the bubble as a function of N, V, and T, and can determine all of the partial derivatives necessary to calculate $\dot{T}$.

The specific heat per water molecule c_v is plotted versus temperature for several values of the pressure in Fig. 3.

IV. BLACKBODY RADIATION

Thermal radiation, which is strongly dependent on the temperature of the system, can be an important contribution to the energy partition of the underwater spark. In a naive model of the gas globe as a perfect blackbody radiator, thermal radiation represents a power loss proportional to the fourth power of the temperature as described by the Stefan–Boltzmann law,

$$\dot{Q}_b = 4\pi R^2 \sigma T^4, \quad (39)$$

where σ is the Stefan–Boltzmann constant. This corresponds to an electromagnetic flux S normal to the surface of the gas globe of

$$S = \sigma T^4. \quad (40)$$

In a less naive approach we modify the Stefan–Boltzmann law by including the emissivity ϵ of the bubble. The equation for the flux normal to the bubble surface is replaced by

$$S = \epsilon \sigma T^4, \quad (41)$$

with $0 \leq \epsilon \leq 1$.

In this section we use the time-dependent radiative transfer equation (RTE)[3,4,15,16] to calculate the emissivity by calculating the flux normal to the bubble surface as a function of the thermodynamic quantities of the system, i.e., pres-
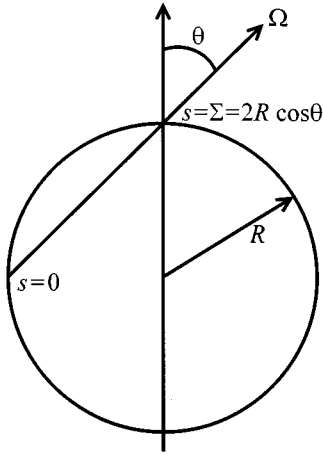
FIG. 4. A representative light ray in the geometry of a sphere. The path length of the light ray through the bubble is represented by s with a total path length of $\Pi = 2R \cos \theta$.

sure and temperature, and the geometry of the bubble, i.e., its radius and spherical shape. The approach we use is to calculate the solutions to the RTE, integrating them over solid angle and frequency to arrive at the flux normal to the surface.

The flux at a point on the surface of the body $\mathbf{r}$ in the $\mathbf{n}$ directions is composed of the $\mathbf{n}$-component of the intensity of light rays $I(\mathbf{r},\mathbf{\Omega})$ emerging from all angles $\mathbf{\Omega}$ within the body,

$$S(\mathbf{r},\mathbf{n}) = \int_{2\pi} I(\mathbf{r},\mathbf{\Omega}) \mathbf{n} \cdot \mathbf{\Omega} \, d\mathbf{\Omega}, \tag{42}$$

where the integral is taken over the emerging hemisphere. A representative light ray in a spherical geometry is shown in Fig. 4, and the integration for this geometry is

$$S(\mathbf{r},\hat{\mathbf{r}}) = 2\pi \int_0^{\pi/2} I(\mathbf{r},\theta) \cos \theta \sin \theta \, d\theta. \tag{43}$$

The intensity of each light ray is composed of the spectral intensities I_ν from all photon frequencies in the electromagnetic spectrum,

$$I(\mathbf{r},\mathbf{\Omega}) = \int_0^\infty I_\nu(\mathbf{r},\mathbf{\Omega}) d\nu. \tag{44}$$

The spectral intensity can be calculated at any point in space by solving the time-independent radiative transfer equation

$$\mathbf{\Omega} \cdot \mathbf{\nabla} I_\nu(\mathbf{r},\mathbf{\Omega}) = \kappa_\nu'(T,P)(I_{\nu p}(T) - I_\nu(\mathbf{r},\mathbf{\Omega})), \tag{45}$$

where $I_{\nu p}$ is Planck's expression for the intensity of a light beam in a system in radiative equilibrium at temperature T,

$$I_{\nu p}(T) = \frac{2h\nu^3}{c^2} \frac{1}{e^{h\nu/kT} - 1}, \tag{46}$$

and κ_ν' is the effective absorption coefficient for the gas at a given temperature and pressure. The effective absorption coefficient is related to the actual absorption coefficient κ_ν by

$$\kappa_\nu'(T,P) = \kappa_\nu(T,P)(1 - e^{-h\nu/kT}). \tag{47}$$

Since we model the temperature and pressure as uniform within the bubble, κ_ν' is a constant along any light beam; therefore Eq. (45) can be solved analytically along a path of length Σ, such as that shown in Fig. 4,

$$I_\nu(\Sigma,\mathbf{\Omega}) = I_{\nu p}(1 - e^{-\kappa_\nu'\Sigma}). \tag{48}$$

It is important to remember the temperature and pressure dependence of I_ν through $I_{\nu p}(T)$ and $\kappa_\nu'(T,P)$.

The angular dependence of I_ν is contained within the choice of light ray and its length Σ. By looking again at Fig. 4, we determine that Σ depends on the radius of the sphere and the angle θ between the ray and the normal to the surface,

$$\Sigma = 2R \cos \theta. \tag{49}$$

By integrating over a solid angle, as in Eq. (43), before integrating over photon frequencies, we can obtain an analytical form for the spectral flux normal to the surface of the bubble,

$$S_\nu(R,T,P) = \pi I_{\nu p}\left(1 - \frac{1}{2\tau_\nu'^2}(1 - (1 + 2\tau_\nu')e^{-2\tau_\nu'})\right), \tag{50}$$

where we have defined the effective spectral optical thickness of the sphere τ_ν' by

$$\tau_\nu'(R,T,P) = R\kappa_\nu'(T,P). \tag{51}$$

In the equation for S_ν we have replaced the position $\mathbf{r}$ with the radius R and have dropped the normal $\mathbf{n}$, since we are assuming spherical symmetry.

A perfect blackbody has either infinite extent, $R = \infty$, or infinite absorption, $\kappa_\nu' = \infty$, over all frequencies. In either case the effective spectral optical thickness for the body becomes infinite, and the spectral flux normal to the body becomes independent of geometry

$$\lim_{\tau_\nu' \to \infty} S_\nu = S_{\nu p} = \pi I_{\nu p}. \tag{52}$$

The expression

$$\frac{S_\nu}{S_{\nu p}} = \left(1 - \frac{1}{2\tau_\nu'^2}(1 - (1 + 2\tau_\nu')e^{-2\tau_\nu'})\right) \tag{53}$$

is plotted versus τ_ν' in Fig. 5. This plot shows how deviations from a perfect blackbody, $\tau_\nu' = \infty$, affect the spectral flux.

The final step in the calculation of the flux at the surface of a uniform sphere is the integration over photon frequencies,

$$S(R,T,P) = \int_0^\infty S_\nu(R,T,P) d\nu. \tag{54}$$

This last integral must be performed numerically since the dependence of κ_ν on ν is very complicated.

There are three types of mechanisms pertaining to the absorption and readmission of radiation in hot gases:[15,15] free–free transitions, bound–free transitions, and bound–bound transitions. Each of these mechanisms contributes to the value of the absorption coefficient κ_ν for the medium. We have included free–free and bound–free atomic transitions
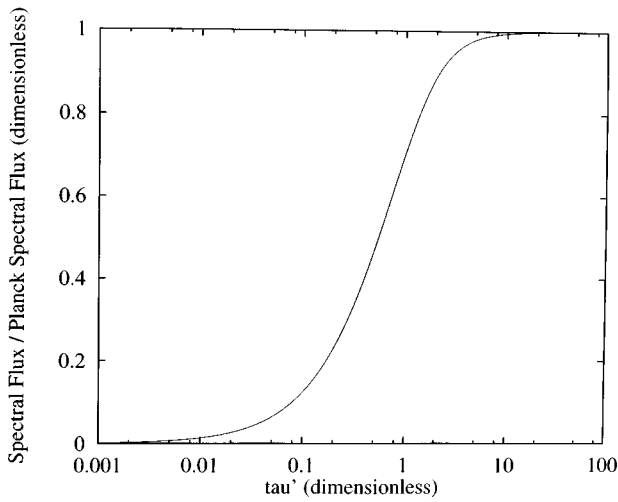
FIG. 5. The spectral flux of a uniform sphere divided by the Planck spectral flux versus effective spectral optical thickness τ'.

FIG. 6. The emissivity versus time after breakdown for the simulation of the sea data discharge.

in our calculations of κ_ν. Bound–bound transitions have not been included due to the computational difficulty they impose,[16] though they are a possibly significant contribution to the absorption.[16–18] We have also omitted molecular transitions in this model since the bubble significantly radiates blackbody radiation only at temperatures where the gas has already completely dissociated.

Additionally, we have assumed that hydrogenlike atoms would be the major contribution to the absorption coefficient; therefore, the hot gas is chosen, for the purpose of calculating κ_ν, as composed of three hydrogen atoms ($Z=1$) for every water molecule, one for each atom in H_2O. Using the formulas from Zel'dovich and Raizer[15] for both the free–free (bremsstrahlung) and the bound–free atomic transitions, we arrive at a formula for the absorption coefficient,

$$\kappa_\nu = \frac{64\pi^4}{3\sqrt{3}} \frac{e^{10} m_e Z^4 N}{h^6 c \nu^3} \left\{ \sum_{n=n*}^{\infty} \frac{1}{n^3} e^{-(x_1 - x_n)} + \frac{e^{-x_1}}{2x_1} \right\}. \tag{55}$$

In this equation the following definitions were used:

$$x = \frac{h\nu}{k_B T}, \tag{56}$$

$$x_1 = \frac{I_H Z^2}{k_B T}, \tag{57}$$

$$x_n = \frac{x_1}{n^2}, \tag{58}$$

$$I_H = \frac{e^4 m_e}{8h^2}, \tag{59}$$

and $n*$ represents the lowest electronic state which can be excited to the continuum by a photon of energy $h\nu$. The I_H term is the first ionization energy of hydrogen, i.e., the difference in energy levels between the ground state and first excited state of hydrogen, $I_H = 13.6$ eV.

We have run the emissivity model over a range of temperatures, pressures, and radii representative of the conditions within our simulations. In this region where the bubble
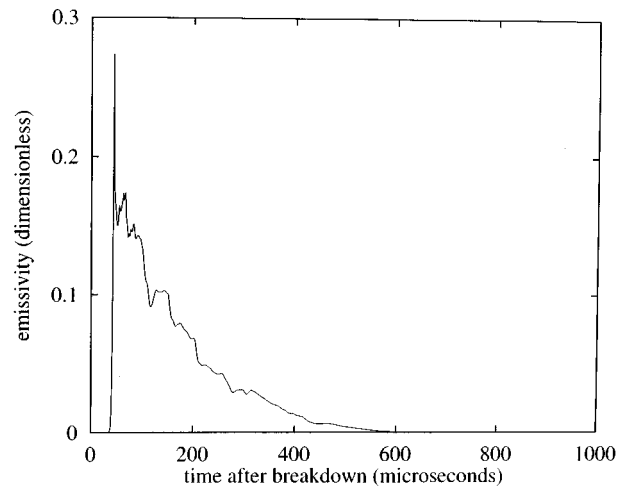
has a radius of roughly 0.03 m, a temperature of 10 000 K and a pressure of 300 atm the emissivity is less than 0.3. As expected, the emissivity increases with increasing bubble radius, temperature, and pressure. There is a pronounced increase in the emissivity as the temperature increases past 10 000 K. Results of the emissivity for a typical simulation are shown in Fig. 6.

V. ABLATION OF THE BUBBLE WALL

When blackbody radiation is emitted from the bubble it is absorbed into the surrounding water, heating the water to a point where it is no longer a liquid, but a gas. This gas mixes with the bubble, increasing the amount of matter within it.

In this ablation model the bubble wall will be treated as a planar surface. Later, we will include spherical spreading effects on the radiant energy density due to an expanding or contracting bubble.

Radiation impinges on the bubble wall, absorbing into the water, as shown in Fig. 7. At some time t the energy density of the absorbed radiation $\mathscr{E}$ at the surface reaches a critical value $\mathscr{E}_\nu$ that defines the transition from liquid water to vapor. At some finite time later, cf. Fig. 7, the energy density will have increased throughout the water so that the
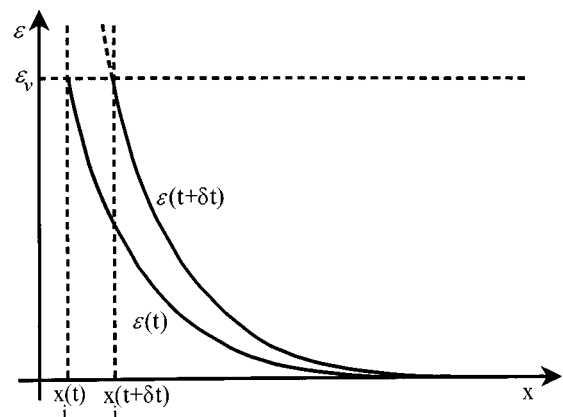

FIG. 7. The ablation process in time step δt.

energy density becomes equal to the critical energy density a distance x_i from the bubble wall. From this distance to the bubble wall, all of the water will have become vapor, and the new liquid–vapor interface will have moved to x_i. By deriving an expression for $\dot{x}_i$, the rate at which the liquid–vapor interface moves, we can determine the rate of water added to the bubble,

$$\dot{N} = 4\pi R^2 \dot{x}_i n_w. \tag{60}$$

The flux of radiation impinging on the bubble wall is determined from Sec. IV to be

$$S_0(t) = \epsilon(T(t), P(t))\sigma T^4(t). \tag{61}$$

This radiation is absorbed into the water surrounding the bubble so that the flux at a depth x into the water is given by

$$S(x,t) = S_0 e^{\alpha(x_i(t)-x)}, \tag{62}$$

where α is the frequency averaged absorption coefficient[3,4] for water. The rate of radiant energy density absorbed at a fixed distance from the bubble wall x is given by

$$\dot{\mathscr{E}}(x,t) = \alpha S_0(t) e^{\alpha(x_i(t)-x)}. \tag{63}$$

Therefore, the radiant energy density absorbed at a given distance is

$$\mathscr{E}(x,t) = \int_0^t \alpha S_0(t') e^{\alpha(x_i(t')-x)}\, dt'. \tag{64}$$

The rate of movement of the liquid–vapor interface can be derived from the condition that energy density at the interface remains at the critical value; in other words, the total time derivative of energy density at the interface is zero,

$$\left.\frac{d\mathscr{E}}{dt}\right|_{x=x_i(t)} = \left(\frac{\partial\mathscr{E}}{\partial t} + \dot{x}\frac{\partial\mathscr{E}}{\partial x}\right)_{x_i(t)} = 0, \tag{65}$$

$$\dot{x}_i(t) = -\left(\frac{\partial\mathscr{E}}{\partial t}\bigg/\frac{\partial\mathscr{E}}{\partial x}\right)_{x_i(t)} \tag{66}$$

$$= \frac{S_0(t)}{\mathscr{E}_v}. \tag{67}$$

With spherical spreading included, the expression for the energy density at a fixed distance and the rate of change of the position of the liquid–vapor interface become

$$\dot{\mathscr{E}}(x,t) = \alpha S_0(t) e^{\alpha(x_i(t)-x)}[0]2\mathscr{E}(x,t)\frac{\dot{R}(t)}{R(t)} \tag{68}$$

and

$$\dot{x}_i(t) = \frac{S_0(t)}{\mathscr{E}_v} - \frac{2}{\alpha}\frac{\dot{R}(t)}{R(t)}, \tag{69}$$

respectively.

The expression for $x_i(t)$ in Eq. (69) is only true under two conditions: The value of $\mathscr{E}$ at the interface is equal to $\mathscr{E}_v$ and the rate of the energy density at the interface, from Eq. (68) with $x=\dot{x}_i(t)$, is positive; otherwise $x_i(t)=0$. In the model we follow the value of the energy density at the interface to determine $\dot{x}_i$,
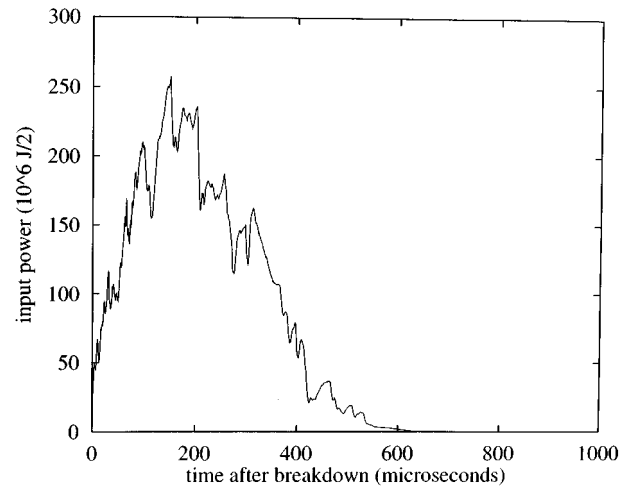

FIG. 8. The input power for the experimental sea data discharge.

$$\dot{\mathscr{E}}(x_i(t),t)$$

$$= \begin{cases} \alpha S_0(t) - 2\epsilon(x_i(t),t)\dfrac{\dot{R}(t)}{R(t)}, & \text{if } \epsilon(x_i(t),t) < \epsilon_v, \\[2mm] 0, & \text{otherwise} \end{cases} \tag{70}$$

and

$$\dot{x}_i = \begin{cases} 0, & \text{if } \mathscr{E}(x_i(t),t) < \mathscr{E}_v \text{ or } \dot{x}_i < 0, \\[2mm] \dfrac{S_0(t)}{\epsilon_v} - \dfrac{2}{\alpha}\dfrac{\dot{R}(t)}{R(t)}, & \text{otherwise.} \end{cases} \tag{71}$$

VI. RESULTS

A. Sea data experiment

The theoretical results discussed in this section will be compared with one spark discharge as an illustration of the properties of the model. This discharge was selected as typical of the hundreds of shots taken over a wide range of energies. See Refs. 3 and 4 for comparisons with other energies and salinity. The experimental data were taken by R. L. Rogers.[2]

This discharge delivered 65 kJ to the sparker at a depth of 73.15 m in the Gulf of Mexico. The input power versus time is shown in Fig. 8 for this discharge, which, although typical of the sea data discharges, was one of the highest energy discharges taken during this experimental run. The acoustic profile was taken by a hydrophone determined to be 19.3 m from the spark source using the time delay from the creation of the spark to the arrival of the impulse. We used both linear and nonlinear propagation codes and found that the differences were not significant in the low-frequency features of the acoustic signature.[3,4] All modeled acoustic profiles for this discharge are propagated to the same distance using linear-acoustic propagation,[3–6]

$$p(r,t) = p_0 + \frac{4\pi\rho_0}{r}\ddot{V}\left(t - \frac{r}{c_0}\right). \tag{72}$$
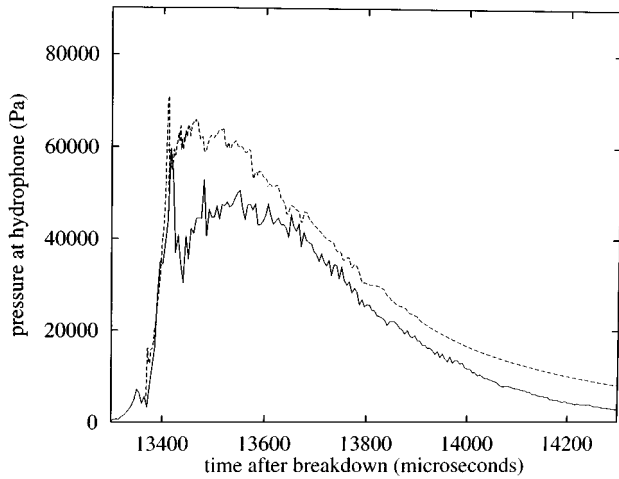
FIG. 9. The acoustic profile for the experimental sea data discharge (solid), compared to calculated acoustic profile (dashed).

Here r is the distance from the spark source to the hydrophone, ρ_0 the ambient mass density, c_0 the ambient speed of sound, and $\dot{V}(t-r/c_0)$ the volume acceleration of the bubble at the retarded time, $t-r/c_0$. The experimental acoustic profile is plotted along with the modeled acoustic profile in Fig. 9.

The only free parameters within the simulation were the initial radius and pressure of the bubble. These were determined by a best fit procedure.[3,4] The initial temperature was set to 373 K. For this set of values the calculated acoustic profile best matches the experimental results, including the prominence of the first peak at $t=13\,410$ μs. The resulting best fit values were physically reasonable for the problem.

1. Initial peak

The initial portion of the pressure profile in Fig. 9 shows a sharp peak followed by a more gradually rising pressure maxima. The rise of the sharp initial peak in the acoustic profile is due to the deposition of a large amount of energy into a very small volume. This causes a corresponding rise in temperature and pressure within the bubble. The increased temperature and pressure give rise to a larger emissivity of the bubble and to a sudden rush of particles through the process of ablation. With the sudden flow of *cold* molecules into the hot bubble, the bubble loses energy in order to heat and dissociate the new mass. This in turn causes a sudden decrease in the rate of expansion of the bubble. This sudden decrease in the expansion rate is seen as the sudden downward slope of the acoustic profile. The second slowly rising peak is due to the continued energy deposition into a gas containing a larger number of particles in a larger volume.

Therefore, the effects of blackbody radiation have a significant impact on the character of the acoustic profile due to the quenching by the mass transported into the bubble through the blackbody induced ablation process.

The energy partition for this discharge at 1000 μs after the ignition of the spark is shown in Table III. For energy balance accounting in Tables III and IV acoustic radiation is

TABLE III. The energy partition of the underwater spark for the simulation of the experimental sea data discharge. The energy partition is taken at $t=1000$ μs after the spark ignition.

Spark duration (s)	6.54×10^{-4}
ΔN (molecules)	2.20×10^{22}
Energy in (J)	65 250
Acoust. rad. (J)	4170
Total work (J)	26 180
Internal (J)	39 060
Int. + work (J)	65 240
BB loss (J)	190
$c_{vb}T_b\Delta N$ (J)	340

included in the total work. This mechanism is automatically accounted for by the Kirkwood–Bethe bubble dynamics model.

B. Half-sine power input

An important question for spark source system designs relates to the dependence of the acoustic profile on the shape of the energy discharge. We can extend our calculations of the energy partition to currently unattainable regimes with this model for the underwater spark. But more importantly, by changing the thermal input power to a smoothly varying function of time we can examine the propagated acoustic profile and energy partition for effects due to the underlying physical mechanisms. As one example of this, we will calculate the bubble growth and obtain an energy partition for two sparks with durations τ of 100 and 200 μs, respectively. The input power profile over the duration of the spark will be a one-half cycle of a sine wave, $\dot{Q}(t)=\dot{Q}_0 \sin(\pi t/\tau)$. Each spark delivers 65 000 J to the bubble, the same amount of energy as the sea data discharge delivered in approximately one-sixth and one-thirtieth the time. The acoustic profiles profiles for the two discharges are shown in Fig. 10.

There are three features worth noting in the acoustic profiles: a small shoulder in the initial rise of the peak, the prominent initial spike in the initial rise of the peak, and the slowly rising maxima in the pressure profile. The first small shoulder is due to the dissociation of the water vapor into atomic constituents; this takes place at approximately 4000 K. The large spike in the initial rise is due to the same mechanisms discussed for the sea data discharge. The third feature, the slowly rising maxima in the pressure profile, is due to the continued deposition of energy into a gas that contains a larger number of particles. The specific heat

TABLE IV. The energy partition of the underwater spark for the simulation of the half-sine power discharge function. The energy partition is taken at $t=1000$ μs after the spark ignition.

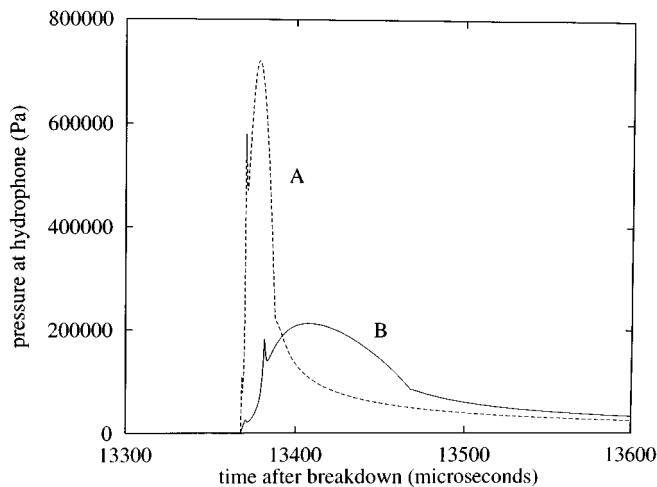|		
Spark duration (s)	1.00×10^{-4}	2.00×10^{-5}
ΔN (molecules)	2.19×10^{22}	2.23×10^{22}
Energy in (J)	65 060	65 060
Acoust. rad. (J)	10 290	22 850
Total work (J)	33 790	38 180
Internal (J)	30 590	24 530
Int. + work (J)	64 380	62 710
BB loss (J)	170	160
$c_{vb}T_b\Delta N$ (J)	340	350

FIG. 10. The acoustic profile for 65 000-J half-sine power inputs with durations of (a) 20 and (b) 100 μs.

climbs steeps at this temperature, which means that the deposited energy is going into the dissociation of the vapor instead of work on the surrounding water.

In the parameter regimes we have studied we have found no similar peak associated with the ionization phase transition within the gas. As we have shortened the spark duration, both the temperature and the pressure increase within the bubble. As the temperature increases to the point where the ionization plays an important role in the energy balance, two phenomena join to counteract the effect of ionization. The first is that the increasing pressure in the bubble moves the onset of ionization to higher temperatures, cf. Fig. 3. The second is that when the temperature reaches the onset of ionization, $T \approx 20\,000$ K, the ablation process has already started to quench the system, lowering the temperature rate in the system.

The energy partitions for these discharges at 1000 μs after the ignition of the spark are shown in Table IV.

C. Energy partition

The results of our model have borne out our intuition that the faster energy is pumped into the bubble the more energy is transferred into work, and therefore, acoustic radiation. As we decreased the duration τ of the spark from 600 to 20 μs, for the same amount of energy, the quantity of energy radiated acoustically increased dramatically. Since the amount of total work done by the shorter duration spark does not increase as dramatically as the acoustic radiation, we can surmise that less energy is being stored in the potential energy of the water surrounding the bubble.

The energy partitions in Table IV also reveal an interesting feature of this underwater spark model. Even though the temperature and emissivity of the short duration sparks are much larger than for long duration sparks, the blackbody radiation loss and the number of ablated particles vary little. This is due to the coupled nature of the blackbody ablation model with the thermodynamics model. When the spark raises the temperature of the bubble enough to contribute to blackbody losses, the ablation process floods the bubble with

cold molecules, which lower the temperature and emissivity. This negative feedback mechanism ensures that blackbody radiation losses do not dominate the energy partition.

Even though the actual energy losses due to blackbody radiation are small, the contribution to the dynamics of the bubble growth through the coupled process of ablation makes blackbody radiation a significant physical mechanism within the spark generated bubble. This is most evident when one examines the structure of the initial acoustic peak in both the simulated and experimental data.

VII. SUMMARY AND CONCLUSION

We have developed a model which will enable one to investigate aspects of the underwater spark which cannot be obtained from experimental data. This model enables us to examine the processes within the bubble and establish which mechanisms are responsible for the conversion of energy from the electrical energy of the spark into other channels.

There are aspects of the actual spark generated bubble system which have not been addressed by this model. A rough calculation of the thermal relaxation time for a hot bubble tells us that the assumption of a homogeneous bubble is not accurate. A nonhomogeneous bubble would likely have a very hot central core surrounded by a cooler vapor region. The blackbody radiation from such a geometry could vary significantly from that of the homogeneous bubble. With the tight coupling between the blackbody radiation and ablation mechanisms one would also expect that ablation will also be affected. Further refinements to this bubble model should include heat transport within the bubble along with the variation of temperature and pressure along the radius of the bubble.

Furthermore, Fujikawa and Akamatsu[19] cite significant heat conduction during the collapse phase of the cavitation bubbles in water. Heat conduction comes into play only when the bubble attains very high temperature. In our calculations, as state earlier, ablation effects, which are not included in the above paper, quench the temperature of the system to less than 20 000 K. Thus, in this regime, thermal conduction is never really important.

We have examined the thermodynamics of the bubble system, creating models for dissociation, ionization, blackbody radiation, and ablation processes within the bubble. We have also demonstrated how these processes are interrelated and how they affect the acoustic profile. We may now use this model to explore energy delivery profiles and their effects on the energy partition.

[1] K. A. Naugol'nykh and N. A. Roi, *Elektricheskie Razrjady V Vode* (Nauka, Moskva, 1971) [English translation: ''Spark Discharges in Water,'' Internal Report, Applied Research Laboratories, Austin, Texas, 1987].

[2] R. L. Rogers, Technical Rep. No. ARL-TR-92-15, Applied Research Laboratories.

[3] R. M. Roberts, Ph.D. thesis, The University of Texas at Austin, 1993.

[4] R. M. Roberts, Technical Rep. No. ARL-TR-93-9, Applied Research Laboratories.

[5] J. A. Cook, Ph.D. thesis, The University of Texas at Austin, 1993.

[6] J. A. Cook, Technical Rep. No. ARL-TR-93-10, Applied Research Laboratories.

[7] R. H. Cole, *Underwater Explosions* (Princeton U. P., Princeton, 1948).

[8] J. G. Kirkwood and H. A. Bethe, Technical Rep. No. 588-252, Cornell University.

[9] A. B. Arons, J. P. Slifko, and A. Carter, J. Acoust. Soc. Am. **20**, 271 (1948).

[10] A. B. Arons, J. Acoust. Soc. Am. **20**, 277 (1948).

[11] A. B. Arons and D. R. Yennie, Rev. Mod. Phys. **20**, 519 (1948).

[12] A. Ziolkowski, Geophys. J. R. Astron. Soc. **21**, 137 (1970).

[13] F. R. Gilmore, Technical Rep. No. 26-4, Hydrodynamics Laboratory, California Institute of Technology, Passadena, California.

[14] L. D. Landau and E. M. Lifshitz, ''Statistical Physics,'' Part 1, Vol. 5 of *Course of Theoretical Physics*, 3rd ed. (Pergamon, New York, 1980).

[15] Y. B. Zel'dovich and Y. P. Raizer, *Physics of Shock Waves and High-Temperature Hydrodynamics Phenomena* (Academic, New York, 1966), Vol. I.

[16] R. I. Soloukhin and R. Goulard, *Handbook of Radiative Heat Transfer in High-Temperature Gases* (Hemisphere, Washington, DC, 1987).

[17] L. M. Biberman and A. N. Lagarkov, Opt. Spektrosk. [Opt. Spectrosc. (USSR)] **16**, 173 (1964).

[18] H. R. Griem, Astrophys. J. **136**, 422 (1962).

[19] S. Fujikawa and T. Akamatsu, J. Fluid Mech. **97**, 481 (1980).